Densification of ZrC_x-ZrB_2 Composites by Reactive Hot Pressing at Low Applied Pressure

RAJAGURU KANNAN and LINGAPPA RANGARAJ

Dense ZrC_x-ZrB_2 (10 to 50 vol pct) composites were produced by reactive hot pressing (RHP) of different molar ratios Zr, C, and B powder mixtures at 4 to 7 MPa, 1200 °C for 60 minutes. An applied pressure of 4 MPa was found to be sufficient to produce ZrC_x-ZrB_2 (10 to 20 vol pct) composites with 96 to 97 pct relative density (RD). However, to achieve similar RD with a higher volume of ZrB_2 (≤ 50 vol pct), 7 MPa was required. RHP of the 1.83Zr-0.5C-1.66B powder mixture (50 vol pct ZrB_2) at 600 °C to 1200 °C for 5 minutes illustrated sluggishness of the reaction; the plasticity of Zr played a significant role in densification. Microhardness, indention fracture toughness, and three-point flexural strength of the ZrC_x-ZrB_2 (50 vol pct) composites are 14.7 ± 0.5 GPa, 5.5 ± 0.69 MPa$\sqrt{m}$, and 609 ± 38 MPa, respectively. Improvement in the mechanical properties of the composites is believed to be in distribution of ZrB_2 platelets within the ZrC_x matrix.

https://doi.org/10.1007/s11661-018-4647-7

I. INTRODUCTION

ZIRCONIUM carbide (ZrC) and zirconium diboride (ZrB_2) belong to the group of ultra-high-temperature ceramics (UHTCs) having melting temperatures ≥ 3000 °C, hardness ≥ 20 GPa, and superior thermal and chemical stability. Combination of these materials with silicon carbide (SiC) finds applications in leading edges, nose cone tips, thermal protection systems in re-entry vehicles, and wear-resistant components since they survive severe oxidation and temperatures ≥ 2000 °C. Dense UHTCs, in the form of monoliths and composites, have been produced by various methods, such as pressureless sintering (PS), hot pressing (HP), reactive hot pressing (RHP), and spark plasma sintering, for the last decade. PS of ZrB_2[1] and ZrB_2-SiC composites[2] at ≥ 2000 °C for longer durations results in ≥ 95 pct relative density (RD), whereas pressureless reactive sintering of Zr-2B powder mixture at 2000 °C to 2200 °C for 60 minutes leads to monolithic ZrB_2 with only 65 to 79 pct RD.[3] HP of ZrB_2-Ni,[4] ZrB_2-Si_3N_4,[5] ZrB_2-SiC,[6] and ZrB_2-ZrC[7] at ~ 32 MPa and ~ 1900 °C yields ~ 98 to 99.8 pct RD. RHP of Zr-B_4C, Zr-B-SiC, and Zr-B_4C-Si powder mixtures results in dense ZrB_2-ZrC, ZrB_2-SiC, and ZrB_2-SiC-ZrC composites at 1600 °C to 1900 °C.[8–13] RHP of ZrH_2-2B powder mixture at 35 MPa in the temperature range 1800 °C to 2100 °C results in monolithic ZrB_2 with 88.6 to 99.7 pct RD.[14] Studies show that a judicious choice of starting Zr-B_4C powder mixture composition can reduce the RHP temperature to 1200 °C.[15] The densification in ZrB_2-ZrC_x composites at this temperature is reported to be by the formation of nonstoichiometric ZrC_x at low temperatures.[15] Moreover, drastic reduction of critical resolved shear stress in this nonstoichiometry significantly affects densification. Subsequently, this has been further confirmed by RHP at 1200 °C to 1600 °C for monolithic ZrC_x with different molar ratios of Zr:C.[16] Studies have also shown that RHP of 2Zr-B_4C-Si and 3.5Zr-B_4C-SiC powder mixtures at 1400 °C to 1600 °C results in final products with ZrB_2-SiC and ZrB_2-ZrC_x-SiC composites.[17,18]

The outcome of these reports is that RHP is significantly dependent on the application of pressure during the schedule. In all the aforementioned reports, the pressure application starts in the temperature range of 1400 °C to 1600 °C[9–12] or after the final temperature has been reached,[13,19] resulting in incomplete densification. Such a decompression is due to the reaction in the powder compact being almost complete within the temperature range of 1600 °C to 1900 °C,[9–14,19] leading to a compact with a network of pores. Further, densification in these compacts can occur only on application of substantial pressure and subsequent HP.[4–7] In this respect, transient plastic phase processing (TPPP) is advantageous[20,21]; transient plastic phases, such as nonstoichiometric carbide, play a crucial role in densification.

The selection of a suitable starting powder composition and application of pressure at ~ 950 °C during RHP results in dense ZrB_2-ZrC_x[15]/ZrC_x[16] and ZrB_2-

RAJAGURU KANNAN and LINGAPPA RANGARAJ are with the Materials Science Division, CSIR-National Aerospace Laboratories, Bengaluru 560017, India and also with the Academy of Scientific and Innovative Research, CSIR-NAL Campus, Bengaluru 560017, India. Contact email: ranga@nal.res.in

Manuscript submitted October 13, 2017.
Article published online May 14, 2018

ZrC_x-SiC[18] at 1200 °C and 1400 °C, respectively. Enhanced densification during RHP is attributed to the formation of transient and deformable ZrC_x phase. Most recently, two-stage RHP experiments conducted at 40 MPa and 800/1200 °C on Zr + C powder mixtures with different molar fractions of Zr:C showed that the volume fraction of Zr in the powder mixture played a significant role in the densification of the compacts.[22,23] A detailed study indicated that the Zr metal-rich Zr + C powder mixtures (corresponding to $ZrC_{0.5}$ and $ZrC_{0.67}$) densified at pressures as low as 4 to 10 MPa and a temperature of 1200 °C for 60 minutes[24]; the densification occurred due to the presence of residual Zr ≥ 1000 °C, which significantly changed the yield stress from 30 MPa at 800 °C to 2 MPa at 1100 °C.[25–27]

It is now well established that Zr + C powder mixtures corresponding to nonstoichiometric ZrC_x can densify at low temperatures and pressures; the densification is mainly due to plasticity of the Zr metal at low temperatures and that of the ZrC_x phase at elevated temperatures.[24] However, the strength and oxidation resistance of these monolithic ceramics are not adequate for satisfactory applications. One of the ways for improving these properties is to incorporate ZrB_2 phase in the ZrC_x matrix. In this study, an attempt has been made to fabricate ZrC_x-ZrB_2 composites from elemental Zr-C-B powder mixtures by RHP at low pressures and moderate temperatures. The composition of the powder mixtures was varied to obtain composites of ZrC_x-ZrB_2 (0 to 70 vol pct) with satisfactory mechanical properties.

II. EXPERIMENTAL

A. *Preparation of Powder Mixtures*

The three starting powders used in the present study were zirconium (Zr): ~ 98 pct pure (Hf 1 pct), 2- to 10-μm particle size (M/s Yashoda Special Metals, Hyderabad, India); graphite (C): ~ 99 pct pure, 7- to 10-μm particle size (M/s Alfa Aesar, Ward Hill, MA); and amorphous boron (B): ~ 97 pct pure (M/s Sigma-Aldrich). The powder mixtures with varying mole fractions of elemental constituents were selected to obtain ZrC_x-ZrB_2 (0 to 70 vol pct) composites per Reaction [1]. In the remaining part of the text, these samples are referred to as monolithic ZrC_x and ZCB-X (where X = 10 to 70 vol pct ZrB_2 phase with an interval of 10 vol pct). For example, ZCB-10 relates to the powder mixture, which, upon completion of the reaction, would result in a ZrC_x-ZrB_2 composite with 10 vol pct ZrB_2 phase. Monolithic ZrB_2 was also processed using 1 mol of Zr and 2 mol of B.

$$(1+x)\mathrm{Zr} + 0.5\mathrm{C} + 2x\mathrm{B} \rightarrow \mathrm{ZrC}_{0.5} + x\mathrm{ZrB}_2 (x = 0 \text{ to } 1.925) \quad [1]$$

Starting molar ratios, volumetric compositions, Gibbs free energy of formation, theoretical densities of powder mixtures, expected phases and their volumetric contents, and theoretical densities of monolithic $ZrC_{0.5}$ and ZCB-X composites are summarized in Table I. The theoretical densities were calculated according to the rule of mixtures based on the densities of 6.5, 2.27, 2.37, 6.37, and 6.1 g/cm^3 for Zr, C, B, $ZrC_{0.5}$,[16] and ZrB_2, respectively. For preparation of the powder mixtures, constituent elemental powders were taken per the weight percentage listed in Table I. The powders were mixed in ethanol with ZrO_2-Y_2O_3 (8 mol pct) milling media for 24 hours in a plastic bottle using a horizontal rotary ball mill and dried at 100 °C for 60 minutes. Differential thermal analysis/Thermogravimetric analysis (DTA/TGA, Netzsch STA 409PC, Germany) was carried out on the powder mixtures of Zr-0.5C, Zr-2B, ZCB-30, ZCB-50, and ZCB-70 for determining the onset temperatures for the reactions. The experiments were carried out up to 1250 °C at a heating rate of 10 °C/min under a continuous flow of high-purity argon gas.

B. *Reactive Hot Pressing*

The dried powder mixture was filled in the hardened steel die with 30-mm inner diameter and cold compacted at 50 MPa. The green density of the sample was calculated by measuring the diameter, thickness, and weight. The green compact was placed in a high-density graphite die (30.4: inner diameter and 60 mm: length); direct contact between the powder compact and the die top-bottom plungers was avoided by placing a 0.2-mm-thick graphite foil. RHP experiments were carried out at 1200 °C for 60 minutes using a laboratory-designed hot press under a flowing argon atmosphere. The reaction of the transition metals (Ti, Zr) with B/C/nitrogen (N) or boron carbide (B_4C)/boron nitride (BN) is highly exothermic; hence, at rapid rates of heating, the thermodynamic conditions are satisfied for a self-sustaining combustion process.[28] Since the self-sustaining reaction is not desirable during RHP from the densification point of view, the heating rate lower than 10 °C/min was employed. In the present set of experiments, the heating rate of 5 °C/min to 6 °C/min was maintained, and this was selected based on earlier studies by the present authors.[22–24] A pressure of 4 to 7 MPa was maintained on the samples throughout RHP. Following RHP, the furnace was cooled to room temperature at a rate of 8 °C/min, and the pressure on the compact was released on attaining the room temperature. To have a better insight into the reaction process and densification behavior of the composites, RHP of a typical powder mixture corresponding to composition ZCB-50 (1.83Zr-0.5C-1.66B) was carried out under 7 MPa pressure in the temperature range 600 °C to 1200 °C for 5 minutes.

C. *Characterization*

The reactive hot-pressed samples were ground and polished using SiC abrasive papers with decreasing grit size. The final polishing was carried out using 1-μm diamond paste. Density measurement was made by the Archimedes method. X-ray diffraction (XRD) was performed on the flat surface of the samples using Cu K_α radiation (Bruker X-ray diffractometer, operated at 40 kV) for identification of phases. Quantification of product phases and unreacted phases, if any, in the

Table I. Starting Compositions, Volume Percentage, Gibbs Free Energy of the Formation, the Density of Starting Powder Mixture, the Density of Green Compacts, Expected Volume Percentage, and Theoretical Density of Composites

Starting Molar Composition	Volume (Weight) Percentage of Starting Composition			ΔG at 25 °C (kJ/mol)	Theoretical Density of Powder Mixture (g/cm^3)	Density of Green Compacts (g/cm^3)	Expected Volume Percentage of Phases after RHP		Theoretical Density of Composites by Rule of Mixture (g/cm^3)
	Zr	C	B				$ZrC_{x-0.5}$	ZrB_2	
Zr-0.5C[24]	84	16	—	−113.5 ± 10	5.85	3.64	100	—	6.37
1.092Zr-0.5C-0.186B: ZCB-10	81.4 (92.55)	14 (5.56)	4.6 (1.88)	−134.0 ± 9	5.72	3.59	90	10	6.34
1.207Zr-0.5C-0.414B: ZCB-20	78.6 (91.31)	12.3 (4.98)	9.1 (3.71)	−154.4 ± 8	5.61	3.49	80	20	6.31
1.354Zr-0.5C-0.708B: ZCB-30	76 (90.05)	10.6 (4.38)	13.3 (5.56)	−174.9 ± 7	5.51	3.43	70	30	6.29
1.83Zr-0.5C-1.66B: ZCB-50	71.08 (88.76)	7.33 (3.77)	21.59 (7.47)	−215.8 ± 5	5.31	3.29	50	50	6.23
2.24Zr-0.5C-2.48B: ZCB-60	68.73 (87.45)	5.79 (3.15)	25.48 (9.40)	−236.3 ± 4	5.22	3.19	40	60	6.21
2.925Zr-0.5C-3.85B: ZCB-70	67.01 (84.85)	4.32 (1.91)	28.67 (13.24)	−256.8 ± 3	5.13	3.13	30	70	6.18
Zr-2B	60.6 (80.84)	—	39.4 (19.16)	−322	4.87	2.61	—	100	6.1

reactive hot-pressed compacts was carried out by "Materials Analysis Using Diffraction" software by the Rietveld analysis method. A DILOR-JOBIN-YVON-SPEX integrated micro-Raman spectrometer (Model Labram) was used to identify the amorphous boron and graphite; microhardness measurement was performed using a Vickers hardness tester (model HSV-20, Shimadzu Co., Kyoto, Japan) at a load of 500 g (4.9 N) with a holding time of 15 seconds. Indentation fracture toughness (K_{IC}) was determined by measuring the radial crack lengths on samples at a test load of 10,000 g (98 N). The empirical relationship proposed by Niihara *et al.*[29] was used to calculate the K_{IC} of the samples. For the microhardness and indentation fracture toughness, 10 measurements were made on each sample and the average values are reported.

The specimens of 25 mm (length) × 3 mm (width) × 2 mm (thickness) in size were sectioned from the reactive hot-pressed disc by electrodischarge machining. Surfaces of the specimens were flattened and the edges chamfered using 600-grit SiC abrasive paper. Flexural strength was measured at room temperature by the three-point bend test (span length of 20 mm) using a Universal testing machine (M/s Instron E3000) with a crosshead speed of 0.5 mm/min. Microstructural and fractography studies on the reactive hot-pressed samples were carried out using a field emission-scanning electron microscope (FE-SEM: Carl Zeiss, Germany).

III. RESULTS

In this section, the reaction and phase analysis is first reported, followed by the densification, microstructural analysis, and mechanical properties.

A. *Differential Thermal Analysis*

Figure 1 shows the DTA plots of Zr-0.5C, Zr-2B, ZCB-30, ZCB-50, and ZCB-70 powder mixtures carried out at 1250 °C. Both Zr-0.5C and Zr-2B powder

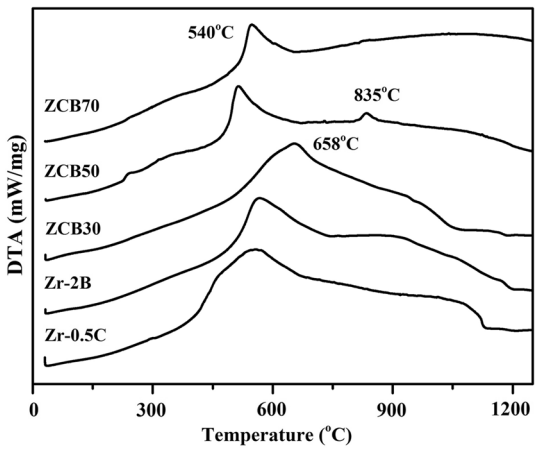

Fig. 1—DTA of Zr-0.5C, Zr-2B, ZCB-30, ZCB-50, and ZCB-70 powder mixtures at 1250 °C.

mixtures showed an exothermic peak with the maximum intensity at ~ 540 °C. It is important to note that the reaction in the Zr-0.5C powder mixture showed a broad peak, whereas the Zr-2B powder mixture showed a sharp peak. The addition of boron to the Zr-0.5C powder mixture did not change the nature of the reaction peak for the ZCB-30 composition, but it slowed the reaction rate. However, further increase in boron addition resulted in the reappearance of the sharp reaction peak with a shift in the reaction temperature to lower temperatures (ZCB-50). For the powder mixture ZCB-70, the reaction behavior is found to be very similar to that of the Zr-2B powder mixture.

B. *XRD Analysis*

Figures 2(a) through (d) show XRD patterns of the monolithic $ZrC_{0.5}$ ceramic, ZCB-10, ZCB-20, and ZCB-30 composites, respectively, reactive hot pressed at 4 MPa and 1200 °C for 60 minutes, while Figures 2(e) through (h) show the XRD patterns of ZCB-50, ZCB-60, ZCB-70, and ZrB_2, respectively, reactive hot pressed at 7 MPa and 1200 °C for 60 minutes. In $ZrC_{0.5}$ (Figure 2(a)), the presence of a small quantity of residual Zr (~ 0.5 vol pct) can be seen.[24] In contrast, RHP of Zr-2B powder mixture showed peaks of ZrB_2 with a small peak of ZrO_2, without residual Zr (Figure 2(h)). It is, however, important to note that the powder mixtures always contain some amount of oxygen either adsorbed on the surface of the particles or as a compound; hence, the presence of a small quantity of ZrO_2 in the reactive hot-pressed ZrB_2 compact is not unusual. The presence of residual Zr in ZCB-10 composite (Figure 2(b)) is ~ 2.5 vol pct. However, it can be noticed that as the boron content in the powder mixture increases, the quantity of residual Zr reduces and the peak intensity of the ZrB_2 phase increases (Figures 2(c) through (g)).

Figure 3 shows XRD patterns of the ZCB-50 composition (1.83Zr-0.5C-1.66B), reactive hot pressed at 7 MPa, in the temperature range of 600 °C to 1200 °C for 5 minutes. The patterns of the starting powder mixture (Figure 3(a)) and the sample reactive hot pressed at 600 °C (Figure 3(b)) are almost similar. Residual boron in the XRD patterns could not be traced due to its amorphous nature. A small quantity of ZrB_2 phase is found in the compact reactive hot pressed at 800 °C (Figure 3(c)). ZrC_x phase in the composite could be detected only when the RHP temperature was 1000 °C (Figure 3(d)). After RHP at 1100 °C, the quantities of ZrB_2 and ZrC_x in the compacts increase with a significant increase in the peak intensities and decrease in residual Zr (Figure 3(e)). Further, on increase in the RHP temperature to 1200 °C, the reaction in the powder mixture almost completes with ZrB_2, ZrC_x, and a negligible quantity of residual Zr (Figure 3(f)). The quantified values of different phases obtained by Rietveld analysis of XRD patterns of reactive hot-pressed composites at various temperatures are summarized in Table II.

The lattice parameter (Table II) of ZrC_x in ZCB-50 after 1000 °C is determined to be 4.688 Å, and it decreased to 4.672 Å after 1200 °C. The lattice parameters a and c of ZrB_2 in ZCB-50 reactive hot pressed at different temperatures are almost similar (Table II). These values are in agreement with JCPDS file 34-0423 (a = 3.169 Å and c = 3.530 Å) and also reactive hot-pressed ZrB_2 at 35 MPa, 1800 °C to 2100 °C.[19]

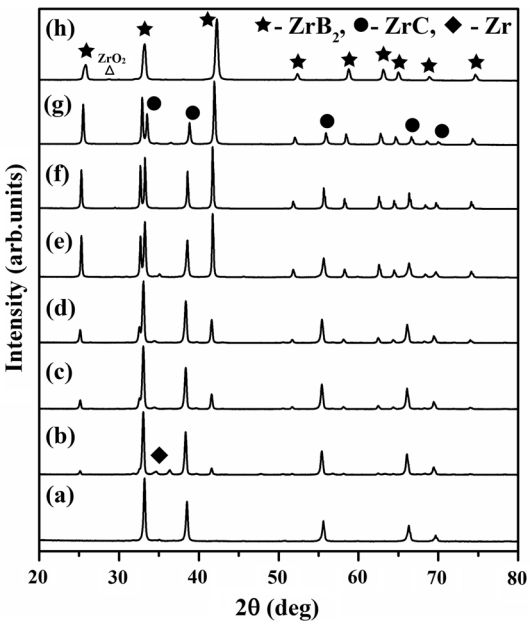

Fig. 2—XRD patterns of reactive hot-pressed samples at 1200 °C for 60 min: (a) monolithic $ZrC_{0.5}$: 4 MPa,[24] (b) ZCB-10: 4 MPa, (c) ZCB-20: 4 MPa, (d) ZCB-30: 4 MPa, (e) ZCB-50: 7 MPa, (f) ZCB-60: 7 MPa, (g) ZCB-70: 7 MPa, and (h) ZrB_2: 7 MPa.

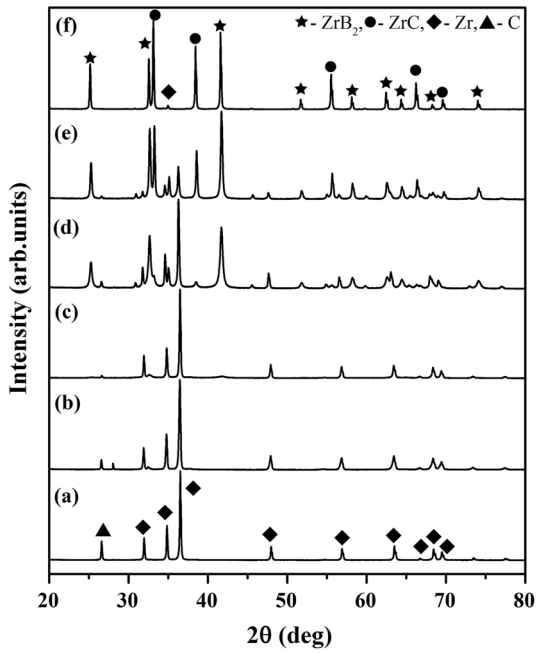

Fig. 3—XRD patterns of ZCB-50 composition reactive hot pressed at 7 MPa for 5 min: (a) starting powder 1.83Zr-0.5C-1.66B, (b) 600 °C, (c) 800 °C, (d) 1000 °C, (e) 1100 °C, and (f) 1200 °C.

Table II. RHP Temperatures, Unreacted, and Product Phases, Lattice Parameter, and Bulk Density of 1.83Zr-0.5C-1.66B (ZCB50) Composition Produced at 7 MPa for 5 Minutes

	Volume Fractions					Lattice Parameter (Å)				
							ZrB_2			
Temperature (°C)	Zr	C	B*	ZrC_x	ZrB_2	ZrC_x *a*	*a*	*c*	Bulk Density (g/cm^3)	Open Porosity (Pct)
RT	71.08	7.33	21.59	—	—	—	—	—	3.29	38
600	48.3	49.9	—	—	1.9	—	—	—	3.22	37.26
800	41.2	47.85	—	—	10.25	—	3.174	3.522	3.55	33.01
1000	23.18	19.62	—	09.15	48.05	4.688	3.170	3.530	3.58	32.52
1100	12.58	3.23	—	27.88	56.32	4.671	3.169	3.530	4.12	16
1200	4	0	—	46.29	49.71	4.672	3.168	3.530	6.02	0.4

*The volume fraction of boron was not considered for calculations due to it being amorphous in nature.

The lattice parameter (Table III) of monolithic ZrC ~ 0.5 is 4.677 Å[24]; it disagrees with the heat-treated ZrC ~ 0.5 at 1800 °C[16] and 1600 °C.[24] However, in the ZCB composites, the decrease in the lattice parameter of ZrC_x from 4.680 Å (ZCB-10) to 4.673 Å (ZCB-70) was observed. The small increase in the lattice parameter in the lower content of ZrB_2 composites may be related to the presence of a small amount of residual Zr. The lattice parameters *a* and *c* of ZrB_2 in ZCB (10 to 30 vol pct) reactive hot pressed at 4 MPa are 3.166 to 3.167 Å and 3.528 to 3.529 Å, respectively. Similarly, those of ZCB (50 to 70 vol pct) reactive hot pressed at 7 MPa are 3.171 to 3.174 Å and 3.531 to 3.534 Å, respectively. The lattice parameters (*a* and *c*) of monolithic ZrB_2 reactive hot pressed at 7 MPa using Zr-2B powder are 3.168 and 3.528 Å.

The volume fractions of ZrC_x, ZrB_2, and residual Zr determined through Rietveld analysis (Table III) are in good agreement with those calculated per the mass balance of the reaction given in Eq. [1] and Table I.

C. *Micro-Raman Analysis*

Figure 4 shows the Raman spectra of ZCB-50 composition reactive hot pressed at 7 MPa and 1000 °C to 1200 °C. It is identified that 550, 823, and 1095 cm^{-1} are distorted amorphous boron (a-boron) with broad and less intense crystalline boron (650 and 730 cm^{-1}) and (1338 and 1580 cm^{-1}) graphite peaks.[30–32] Moreover, a-boron peaks couple with high intense graphite peaks. The transition of a-boron to crystalline boron is perhaps due to the temperature and impurities[32]; even it is not intense and sharp peaks.

The boron and graphite peaks decrease with the increase in temperature from 1000 °C to 1200 °C (Figures 4(a) through (c)). The presence of unreacted boron up to 1200 °C for 5 minutes is illustrated. Further soaking for 60 minutes at 1200 °C shows the completion of reaction without residuals (boron and graphite) of the starting materials (Figure 4(d)).

D. *Densification of the Composites*

The green densities of Zr-0.5C and Zr-C-B powder compacts before RHP are ~ 60 pct of the RD, calculated based on the theoretical density of the individual constituent of the powder mixtures (Table I). The density of the monolithic $ZrC_{0.5}$, reactive hot pressed at 4 MPa and 1200 °C for 60 minutes,[24] is 6.36 g/cm^3 (~ 99 pct RD). The powder mixtures, corresponding to ZCB-10, ZCB-20, and ZCB-30 reactive hot pressed under similar conditions, yielded bulk densities of 6.15, 6.11, and 5.78 g/cm^3 (97, 96, and 92 pct RD), respectively. RDs of the composites were calculated from the measured bulk densities and theoretical densities estimated from the volume fractions of ZrC_x, ZrB_2, and Zr obtained through Rietveld analysis (Table III). The results indicated that the RD of the composites decreased with the increase in ZrB_2 contents. Further, improvement in the densification of these composites is possible only by increasing the applied pressure; by increasing the applied pressure from 4 to 7 MPa during RHP of ZCB-30, an increase in the density from 5.78 to 6.17 g/cm^3 was observed, that is, from 92 to 98 pct RD. A similar trend was observed in the case of ZCB-50 as well. However, in composites with higher ZrB_2 contents ZCB-60 (82 pct RD) and ZCB-70 (68 pct RD), this increase in pressure was observed to be insufficient to enhance the densification process during RHP (Table III).

E. *Microstructural Analysis*

Figure 5, optical micrographs of the ZCB-50 reactive hot pressed at 7 MPa and 1000 °C, 1100 °C, and 1200 °C for 5 minutes, illustrates the densification process. The sample reactive hot pressed at 1000 °C is highly porous with an incomplete reaction in the powder mixture (Figure 5(a)). As the temperature increased to 1100 °C, the density of the compact improved with a considerable decrease in the porosity (Figure 5(b)). The presence of residual Zr metal was observed, as shown in Figures 5(a) and (b). At ~ 1200 °C, a remarkable change in microstructure was observed (Figure 5(c)); the microstructural study shows that significant densification occurred in the compacts in the temperature range 1100 °C to 1200 °C with an applied pressure of 7 MPa. As the holding time increased to 60 minutes, the sample attained almost full density (Figure 5(d)). The color contrast in the figure between the particles ZrB_2 (brown) and ZrC_x (light gray) indicates the formation and distribution of the composite. The final step of the

Table III. Starting Compositions, Pressure, Volume Percentage, Lattice Parameter, Density, RD, Hardness, and Flexural Strength of $ZrC_{0.5}$ and $ZrC_{0.5}$-ZrB_2 Composites

Starting Composition	Pressure (MPa)	Phases (Vol Pct)			Lattice Parameter (Å)			Bulk Density (g/cm^3)	RD (Pct)	Hardness (GPa)	Flexural Strength (MPa)	Average Grain Size (μm)		
						ZrB_2						ZrB_2		
		ZrC_x	ZrB_2	Zr	ZrC	a	c					l	b	ZrC (Dia)
$ZrC_{x-0.5}$[33]	4	99.5	—	0.5	4.677	—	—	6.36	99	13.1 ± 0.5	386 ± 26	—	—	4.2 ± 1.5
ZCB-10	4	88	9.5	2.5	4.681	3.166	3.528	6.15	97	14.5 ± 2.6	445 ± 13	1.60 ± 0.4	0.90 ± 0.5	4.2 ± 1.2
ZCB-20	4	78.2	20.3	1.5	4.681	3.167	3.529	6.11	96	14.3 ± 2.4	317 ± 43	1.58 ± 0.4	0.20 ± 0.2	3.3 ± 1.2
ZCB-30	4	69.8	28.9	1.3	4.680	3.167	3.528	5.78	92	14.7 ± 1.0	230 ± 23	—	—	—
	7	69.7	29.3	1.0	4.679	3.167	3.529	6.17	98	14.6 ± 0.5	489 ± 17	1.31 ± 0.2	0.12 ± 0.1	2.3 ± 0.8
ZCB-50	7	46.2	53.5	0.3	4.679	3.169	3.532	6.07	97	14.7 ± 0.5	609 ± 38	1.01 ± 0.1	0.13 ± 0.1	1.1 ± 0.5
ZCB-60	7	39	61	—	4.673	3.169	3.531	5.12	82	9.1 ± 0.6	287 ± 33	—	—	—
ZCB-70	7	27.2	72.8	—	4.673	3.172	3.534	4.25	68	4.9 ± 1.2	192 ± 15	—	—	—
ZrB_2	7	—	100	—	—	3.168	3.528	2.72	45	—	—	—	—	—

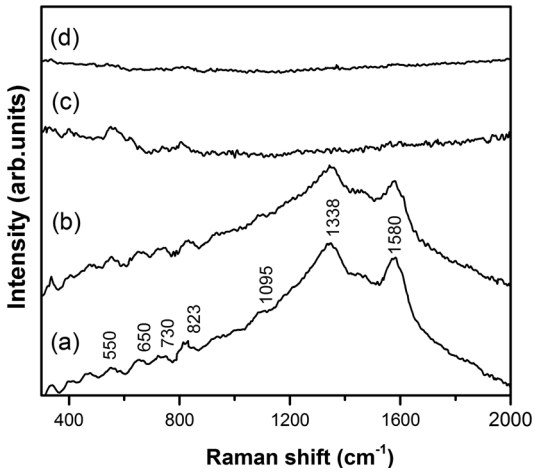

Fig. 4—Micro-Raman spectra of ZCB-50 composition reactive hot pressed at 7 MPa: (a) 1000 °C for 5 min, (b) 1100 °C for 5 min, (c) 1200 °C for 5 min, and (d) 1200 °C for 60 min.

densification mechanism involves connecting grain boundary pores and reduction of pores, as seen in Figure 5(d); *in-situ* formation of ZrB_2 and ZrC_x phases densified at 7 MPa and 1200 °C for 60 minutes is evident.

Figure 6 shows the FE-SEM micrographs of ZCB-10, ZCB-20, ZCB-30, and ZCB-50 composites reactive hot pressed at 4 to 7 MPa, 1200 °C for 60 minutes. In Figure 6(a), light gray regions are the ZrC_x matrix phase, dark gray regions are the ZrB_2 phase, and the white particle is Zr. This residual Zr phase is precisely situated in the grain boundaries of ZrC-ZrC/ZrB_2-ZrB_2/ZrC-ZrB_2, and the increase in boron concentration reduces it. In Figures 6(a) and (b), the ZrB_2 phase randomly disperses within the ZrC_x matrix, and some of the ZrB_2 grains have the shape of platelets. Such a form of the ZrB_2 phase in the microstructure has also been reported in the literature.[8,15,19] An increase of boron concentration in Figures 6(c) and (d) shows that an increasing quantity of ZrB_2 platelets have uniformly distributed in the ZrC_x matrix.

F. *Mechanical Properties*

The results of the microhardness and flexural strength of the $ZrC_{0.5}$ and ZCB composites are summarized in Table III. The microhardness and flexural strength of ZCB-10 and ZCB-20 composites are higher than those of the monolithic $ZrC_{0.5}$.[33] Further increase in ZrB_2 content (ZCB-30) results in a decrease in the flexural strength processed under similar RHP conditions (4 MPa pressure). The reduction of flexural strength is due to the increase of randomly distributed pores (~ 8 pct). The increase of RHP pressure 7 MPa for ZCB-30 and ZCB-50 composites has enhanced flexural strength from 489 ± 17 MPa and 609 ± 38 MPa, respectively.

Figure 7 shows the FE-SEM images of the fractured surfaces of the ZCB-10: 4 MPa, ZCB-20: 4 MPa, ZCB-30: 7MPa, and ZCB-50: 7 MPa composites. The fractured micrograph illustrates the size, shape, orientation, and distribution of the ZrC_x and ZrB_2 phases.

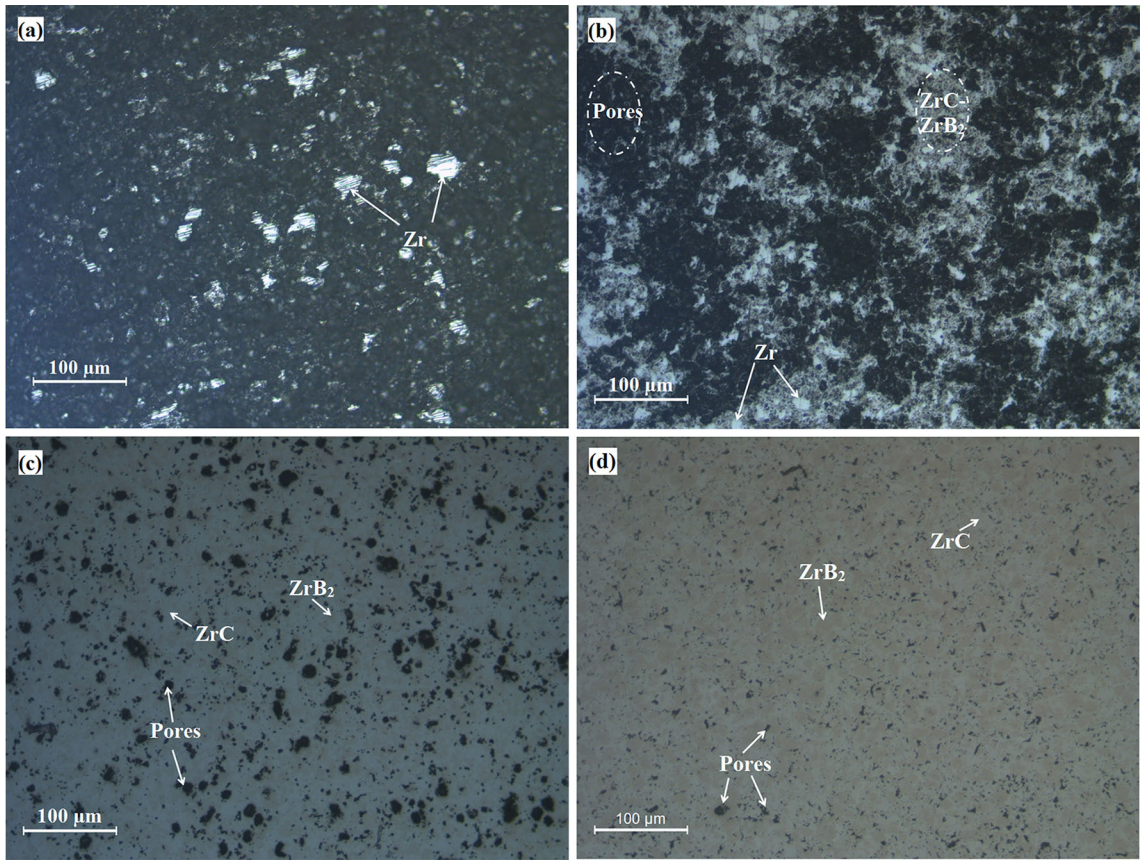

Fig. 5—Optical micrographs of ZCB-50 reactive hot pressed at 7 MPa: (*a*) 1000 °C for 5 min, (*b*) 1100 °C for 5 min, (*c*) 1200 °C for 5 min, and (*d*) 1200 °C for 60 min.

The ZrB_2 platelet morphology and increasing amount of ZrC_x can be seen in ZrC_x-rich composites (Figures 7(a) through (c)). In the ZCB-50 composite (Figure 7(d)), the ZrB_2 platelets are more elongated and ZrC_x grains are smaller than the ZrC_x-rich composites. The average grain sizes of ZrC_x (diameter: 4.2 to 1.1 μm) and ZrB_2 (length: 1.60 to 1.01 μm) were determined and are summarized in Table III. Further, the table confirms the reduction of grain size as an increase in B concentration.

The indentation fracture toughness (K_{IC}) of the ZCB-30 and ZCB-50 composites was measured to be 4.35 ± 0.5 and 5.5 ± 0.69 MPa$\sqrt{m}$, respectively. These K_{IC} values are higher than that of the ZrB_2-ZrC composite produced at 40 MPa and 1600 °C for 4 hours[8] and marginally lower than that of the ZrB_2-ZrC-Zr cermet produced at 20 MPa and 1900 °C for 60 minutes.[19] In the latter case, the fracture toughness is greater because of the presence of $ZrB_2/ZrC_x/Zr$.

IV. DISCUSSION

Emphases on aspects that diverge from some of the earlier reports are discussed in Sections II–A through II–C.

A. *Reaction of Zr-C-B Powder Mixtures*

The addition of a critical content of boron (ZCB-30 and ZCB-50) in the Zr-C powder mixture (Figure 1) illustrates sluggishness of the reaction. Boron addition not only modifies the exothermic reaction (temperature gradient) but also shifts the peak position significantly. These changes are dependent on molar ratios of the reactants in the powder mixture. Thermodynamic calculations carried out per Eqs. [2] through [4] show that entropy and heat of formation of nonstoichiometric $ZrC_{0.5}$ ($S_{Zr\text{-}0.5C} = 31.47$ J/mol and $H_{Zr\text{-}0.5C} = -117.5 \pm 10$ kJ/mol at 25 °C) are less than those of the stoichiometric ZrC ($S_{Zr\text{-}C} = 33.51$ J/mol and $H_{Zr\text{-}C} = -206.6 \pm 10$ kJ/mol at 25 °C).[34–36] Therefore, during heating of the Zr-0.5C powder mixture, it is expected that initially carbon reacts with Zr, resulting in ZrC (4.688 Å at 1000 °C) as the reaction product. After this, residual Zr reacts with ZrC to form $ZrC_{0.5}$ (4.672 Å) at a temperature of 1200 °C. While the former reaction would be highly exothermic, the latter is less exothermic. The resultant would be seen as a broad diffused exothermic peak in the DTA plot, as seen in the present case. This situation arises primarily because of the time-dependent diffusion involved in the reactants during the reaction process.

$$ZrC_x \quad \Delta H_{f,25^\circ C} = 27.97 - 347.4x + 112.8x^2 \pm 10, \quad [2]$$

$$S_{25^\circ C} = 29.43 + 4.08x, \quad [3]$$

$$\Delta G_{f,25^\circ C} = \Delta H_f - T\Delta S, \quad [4]$$

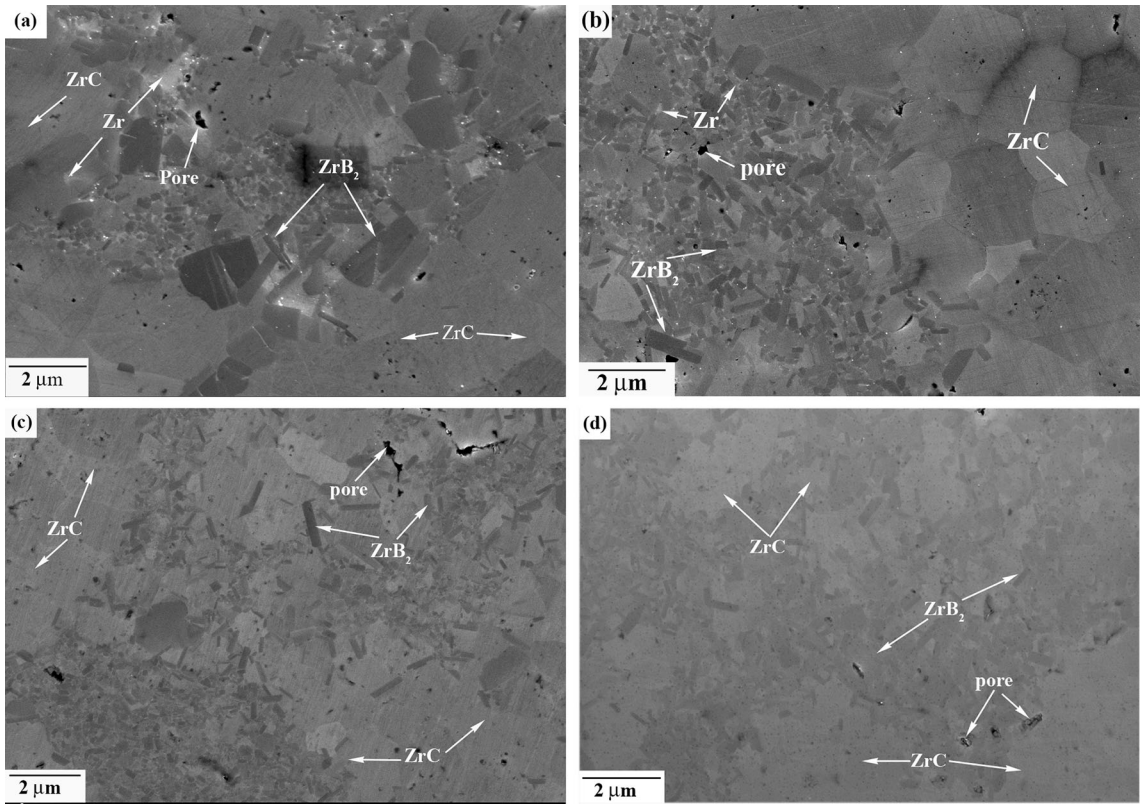

Fig. 6—FE-SEM micrographs of the polished composites reactive hot pressed at 1200 °C for 60 min: (*a*) ZCB-10: 4 MPa, (*b*) ZCB-20: 4 MPa, (*c*) ZCB-30: 7 MPa, and (*d*) ZCB-50: 7 MPa. The light gray is ZrC_x grains, dark gray is ZrB_2 platelets, and white particles are Zr.

where G_f is the Gibbs free energy, H_f is the enthalpy of formation, S is the entropy of the system, and x is the mole concentration of carbon. The ΔG_f at 25 °C for different powder compositions (Table I) is clear evidence for the change in reaction behavior.

From a thermodynamic point of view, the enthalpy of formation (ΔH_f, 25 °C) of ZrB_2 (− 322.6 kJ/mol) is higher than that of ZrC (− 196.7 kJ/mol) and B_4C (− 73 kJ/mol).[35,36] Hence, in a Zr-C-B powder mixture, the reaction would be competitive to form different phases as the temperature increases. In the present case, since the powder mixtures are chosen to give the final products as $ZrC_{0.5}$ and ZrB_2 phases, the balance between the exothermic and reduction of exothermic reactions would determine the nature of the DTA plots (Figure 1). Up to a critical concentration of boron, the broad exothermic peak indicates slowness of the reaction. At a very high concentration of boron, the peak shifts to low temperatures and toward the peak of the pure Zr-B powder mixture. The ZrB_2 and ZrC phases were formed due to the highly exothermic reactions at temperatures < 1000 °C. ZrB_2 is not like Ti-B (multiple phase borides); ZrC has multiple stable phases. Due to this, ZrC_x can modify the exothermic reaction and slow the reaction.

From the XRD (Figure 3) and micro-Raman spectra (Figure 4), it is evident that the reaction progresses slowly during the heating cycle of RHP in the temperature range 600 °C to 1200 °C. Sluggishness of the reaction may be related to the enthalpy of ZrB_2 and ZrC_x. Though the interaction of C-B powder particles is available locally, owing to very low enthalpy of formation, B_4C may not form at these temperatures significantly.[35,37] This can also maintain the residual Zr metal for a long time during RHP. However, the reaction is more or less complete at 1200 °C, which is similar to that reported for RHP of the 3.5Zr-B_4C powder mixture.[15] The lattice parameter of ZrC_x in ZCB-50 produced at 1000 °C indicates that the formation of carbon-rich ZrC occurs at an early stage and later gets converted to nonstoichiometric ZrC_x as the temperature increases to 1200 °C due to the diffusion of residual Zr. The nonstoichiometric ZrC_x is also related to the free energy formation of carbon-rich ZrC_x, which is higher than the Zr-rich ZrC_x. Consequently, a significant quantity of Zr (Figures 3(e) and 5(b)) is later consumed to convert ZrC into nonstoichiometric ZrC_x (Figures 3(f) and 5(c)). It is evident that the selection of starting compositions, especially Zr-rich metal, assists in slowing the reaction during RHP. The micro-Raman spectrum of the ZCB-50 composition is also reflected in the same sluggishness of the reaction related to the presence of boron and graphite at 1000 °C to 1200 °C for 5 minutes. The disappearance of boron and graphite peaks (Figure 4(d)) confirms the completion of reaction at 1200 °C with soaking for 60 minutes.

B. *Effect of Zr on Densification of the Composites*

The densification behavior of Zr-0.5C powder mixture changes with the addition of boron powder. Owing to thermodynamic reasons, the formation of ZrB_2 is

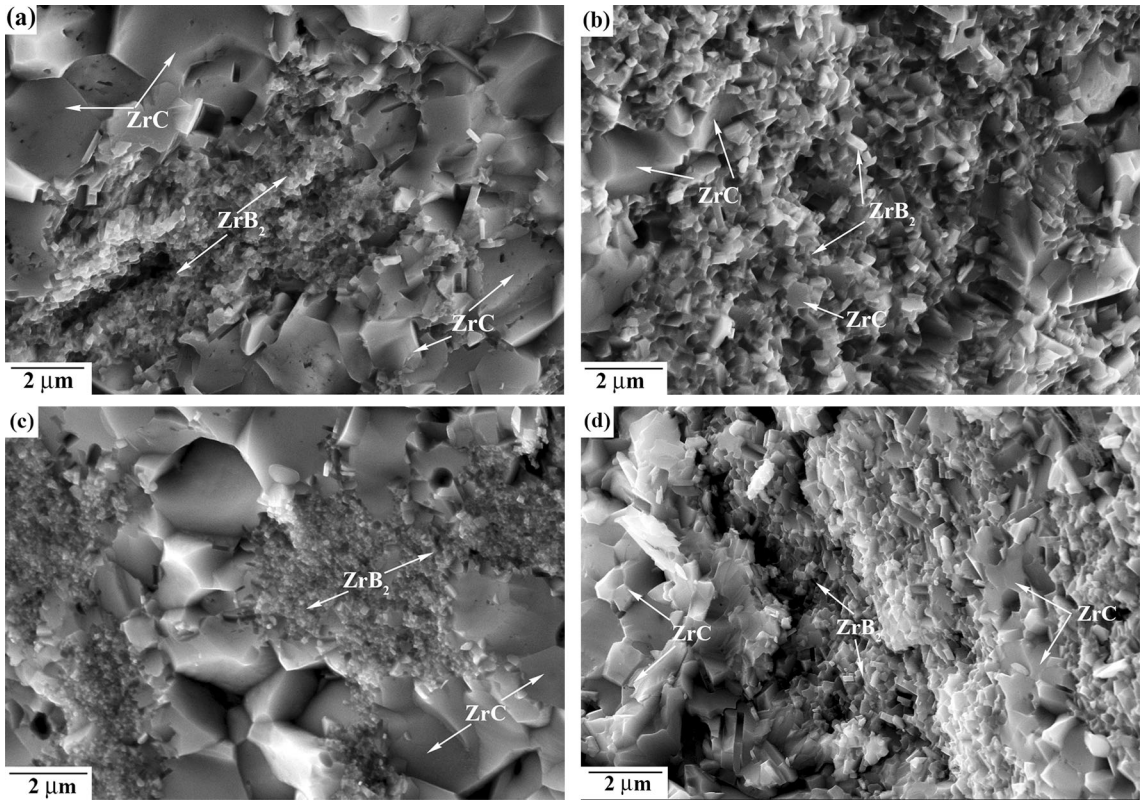

Fig. 7—FE-SEM micrographs of the fractured surfaces of the composites reactive hot pressed at 1200 °C for 60 min: (*a*) ZCB-10: 4 MPa, (*b*) ZCB-20: 4 MPa, (*c*) ZCB-30: 7 MPa, and (*d*) ZCB-50: 7 MPa. ZrB_2 platelet/grain distribution within the ZrC_x matrix can be seen.

Table IV. Starting Composition, Experimental Conditions, Pressure Application Temperature, Phase(s), RD, and Flexural Strength of ZrB_2-ZrC Composites Reported in the Literature

Composition	Process: Experimental Conditions (MPa/°C/Min)	Pressure Application at	Phase(s)	RD (Pct)	Flexural Strength (MPa)
ZrB_2-ZrC (10 vol pct)	HP[7]: 32/1900/45	1600 °C	ZrB_2, ZrC	99	696 ± 82
3Zr-B_4C	two-stage RHP[8]: 40 to 80/800/240 40 to 80/1600/240	before heating schedule	ZrB_2, ZrC	fully dense	293
3Zr-B_4C	RHP[9]: 30/1900/60	1550 °C	ZrB_2, ZrC	98.4	452 ± 45
3Zr-B_4C	RHP[15]: 40/1600/30	1400 °C	ZrB_2, ZrC	96	—
3.5Zr-B_4C	40/1200/30	950 °C	ZrB_2, $ZrC_{0.67}$	98	
Zr-0.67C	RHP[16]: 40/1200/30	950 °C	$ZrC_{0.67}$	99	
(2.2 + *x*)Zr + 0.6B_4C	RHP[19]: 20/1900/60	not reported	ZrB_2, $ZrC_{0.6}$, Zr	99	546 ± 98 (no Zr) 889 ± 44 (15.8 vol pct Zr)
ZrH_2-2B	RHP[14]: 50/1800 to 2100/15 to 45	after reaching final temperature	ZrB_2, ZrO_2	88.6 to 99.7	—

more favorable compared to that of ZrC. In the case of Zr-0.5C powder mixtures, compound formation takes place nonstoichiometrically (ZrC_x). In such a case, the densification by TPPP concurrently with the reaction is significantly prevalent. Hence, the densification of $ZrC_{0.5}$ during RHP is quite useful even at a low applied pressure. However, the addition of boron to the powder mixture resulted in the formation of ZrC_x/ZrB_2 phases. The ZrB_2 phase is relatively hard and does not aid the densification process, as seen in the case of nonstoichiometric ZrC_x. As the ZrB_2 content in the composite increases, it tends to form a rigid network because of the increase in the contiguity, which eventually slows the densification process. Such a thing is more prevalent in ZCB-50, ZCB-60, and ZCB-70 composites than ZCB-10 and ZCB-20. Therefore, the increase in applied pressure in these cases would be required to enhance the densification process, as noticed in the case of ZCB-30

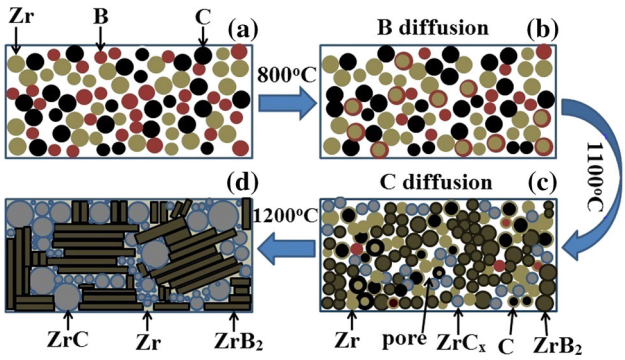

Fig. 8—Schematic sequence of Zr-C-B (ZCB-50) during RHP of reaction and densification: (*a*) starting powder mixture, (*b*) intermediate temperature ~ 800 °C, (*c*) 1100 °C, and (*d*) final temperature at 1200 °C.

and ZCB-50 composites (Table III). However, with higher ZrB_2 contents (ZCB-60 and ZCB-70), still higher pressure or higher temperature (Table IV) is necessary to achieve full densification.[7–9,15,19]

The results of RHP of ZCB-50 powder mixture at different temperatures under an applied pressure of 7 MPa elucidate the densification mechanism. Based on the DTA and XRD plots, the sequence of the reaction and densification process during RHP is proposed schematically in Figures 8(a) through (d). The distribution of Zr, C, and B powders (Figure 8(a)) and RHP at the intermediate stage (≥ 800 °C) illustrates that the formation of ZrB_2 is initiated by the diffusion of boron on the surfaces of Zr particles (Figure 8(b)). The diffusion of B and C into Zr at 1100 °C forms a continuous network between ZrB_2, ZrC_x, and Zr particles, and also isolates the porosity (Figure 8(c)). At the end of the process, the reaction and densification process is completed after attaining the final temperature. Holding the temperature for a long time not only promotes plastic deformation of residual Zr metal that enhances densification, but also results in the reaction between Zr and ZrC to form nonstoichiometric ZrC_x (Figure 8(d)). This can be related to the decrease of Zr yield stress from 30 to ~ 2 MPa when the temperature is increased from 800 °C to 1100 °C.[25–27] The present study exhibits (Table II) that compacts contain a substantial quantity of residual Zr even beyond 1100 °C (Figures 3(e) and 5(b)). Although the volume fraction of elemental Zr decreases as the reaction progresses or RHP temperature increases, the presence of even a small quantity of residual Zr beyond 1100 °C would greatly facilitate the densification process. Therefore, sluggishness of the reaction under the present experimental conditions up to about 1100 °C is beneficial as far as the densification process is concerned. The results indicate that completion of the reaction takes place at a relatively rapid rate when the RHP temperature is in the range 1100 °C to 1200 °C. As the elemental Zr in the compacts gets exhausted or becomes minimal, further densification is governed mainly by creep behavior and the solid-state densification process of the reaction products ZrC_x and ZrB_2. Since plasticity of Zr increases with an increase in temperature, the densification of the compacts continuously takes place under the applied pressure from the beginning of the heating cycle. Earlier reports have confirmed the contributions of Zr metal, in terms of ZrC_x plasticity in densification of ZrB_2-ZrC_x,[15] ZrC_x,[16] and ZrB_2-ZrC_x-SiC[18] compacts during RHP under 40 MPa, when pressure is initiated at ~ 950 °C.

C. *Mechanical Properties of the Composites*

The addition of ZrB_2 into the $ZrC_{0.5}$ matrix increases the hardness from ~ 13 GPa[33] to 14.7 GPa. However, these values are lower than the stoichiometric ZrB_2-ZrC composite.[15] The flexural strength of ZCB-10 produced at 4 MPa is higher than $ZrC_{0.5}$.[33] The flexural strength of ZCB-30 and ZCB-50 produced at 7 MPa is comparatively higher than that of the ZrB_2-ZrC composite (Table IV) produced by RHP at 40 MPa and 1600 °C for 4 hours[8] and 30 MPa and 1900 °C for 60 minutes.[9] The flexural strength values obtained in the present study are almost equivalent to ZrB_2-ZrC-Zr cermets produced by RHP[19] and ZrB_2-ZrC (10 vol pct) composite produced by HP at 1900 °C.[7] The increased flexural strength can also be related to the formation of fine ZrB_2 platelets in the microstructure during RHP due to the dimension restricted by nested ZrC_x/Zr grain boundaries. An increase of boron concentration aids the increase of fine grain structure of ZrC_x/ZrB_2 and platelets (Table III). The incremental boron may be related to the reduction of Zr concentration, which can enhance the grain growth.[19] These fine grains, platelet morphology, orientation of the grains, and residual Zr served in deviating the flexural stress distribution. The microhardness and flexural strength of ZCB-60 and ZCB-70 composites are found to be significantly inferior because of poor densification (Table III). The quantity of ZrB_2 platelet does not just control the improved flexural strength of the ZCB-50 composite (Figures 6(d) and 7(d)); instead, it is the combination of RD and the amount of ZrB_2 platelets in the composite.

RDs and mechanical properties of ZrC_x-ZrB_2 composites fabricated in the present study are comparable to those reported in the literature. However, the novelty of the present study is that the necessary pressure to obtain dense composites is 4 to 7 MPa. This applied pressure is a distinct advantage for processing of dense, large size, and near net shapes.

V. CONCLUSIONS

The present study on RHP of ZrC_x-ZrB_2 composites has led to the following findings.

1. ZrC_x-ZrB_2 (0 to 50 vol pct) composites with 97 to 98 pct RD were fabricated by RHP of elemental Zr-C-B powder mixture at 1200 °C under pressures as low as 4 to 7 MPa. The process was found to be effective in the fabrication of dense composites with ZrB_2 contents up to 50 vol pct at pressure 5 to 10 times less than those reported in the literature.

2. The study indicated that modification of the thermodynamic reaction and densification process during RHP is strongly dependent on the starting Zr-C-B powder mixture compositions. The sluggish reaction during RHP is beneficial, wherein the presence of elemental Zr up to relatively high temperatures (≥ 1100 °C) promotes densification by plastic flow concurrently with other mechanisms.
3. The microhardness (~ 15 GPa), fracture toughness (~ 5.5 MPa$\sqrt{m}$), and flexural strength (609 ± 38 MPa) of the ZCB-50 composites were found to be comparable to those reported in the literature. The fine ZrB_2 platelets in the microstructure and high RD (97 to 98 pct) were responsible for the improved mechanical properties of the composites.

ACKNOWLEDGMENTS

The authors acknowledge the financial support received from the Science and Engineering Research Board, Department of Science and Technology (Project Sanction No. SB/EMEQ-313/2013, dated August 27, 2013), New Delhi, Government of India. The authors thank Dr. S.K. Bhaumik, Head, MSD-NAL, for fruitful discussions during preparation of the manuscript. The authors are thankful to Dr. Anjana Jain, MSD-NAL, for recording XRD patterns; Mr. M. Mahesh, STTD-NAL, for flexural strength measurement; Messrs. Siju and N.T. Manikandanath, SED-NAL, for FE-SEM and Micro-Raman Spectroscopy; and Dr. Padaikathan, Department of Materials Engineering, Indian Institute of Science, Bangalore, for DTA.

REFERENCES

1. A.L. Chamberlain, W.G. Fahrenholtz, and G.E. Hilmas: *J. Am. Ceram. Soc.*, 2006, vol. 89 (2), pp. 450–56.
2. Y. Yan, Z. Huang, S. Dong, and D. Jiang: *J. Am. Ceram. Soc.*, 2006, vol. 89 (11), pp. 3589–92.
3. M. Brochu, B.D. Gauntt, L. Boyer, and R.E. Loehman: *J. Eur. Ceram. Soc.*, 2009, vol. 29 (8), pp. 1493–99.
4. F. Monteverde, S. Guicciardi, and A. Bellosi: *Mater. Sci. Eng. A*, 2003, vol. 346 (1–2), pp. 310–19.
5. F. Monteverde, A. Bellosi, and S. Guicciardi: *J. Eur. Ceram. Soc.*, 2002, vol. 22 (3), pp. 279–88.
6. A.L. Chamberlain, W.G. Fahrenholtz, G.E. Hilmas, and D.T. Ellerby: *J. Am. Ceram. Soc.*, 2004, vol. 87 (6), pp. 1170–72.
7. E.W. Neuman, G.E. Hilmas, and W.G. Fahrenholtz: *J. Am. Ceram. Soc.*, 2016, vol. 99 (2), pp. 597–603.
8. M. Barsoum, A. Zavaliangos, S.R. Kalidindi, T. EI-Ragh, and D. Brodkin: *JOM*, 1995, vol. 47 (11), pp. 52–55.
9. G.J. Zhang, M. Ando, J.F. Yang, T. Ohji, and S. Kanzaki: *J. Eur. Ceram. Soc.*, 2004, vol. 24 (2), pp. 171–78.
10. G.J. Zhang, Z.Y. Deng, N. Kondo, J.F. Yang, T. Ohji, and S. Kanzaki: *J. Am. Ceram. Soc.*, 2000, vol. 83 (9), pp. 2330–32.
11. A.L. Chamberlain, W.G. Fahrenholtz, and G.E. Hilmas: *J. Am. Ceram. Soc.*, 2006, vol. 89 (12), pp. 3638–45.
12. J.W. Zimmermann, G.E. Hilmas, W.G. Fahrenholtz, F. Monteverde, and A. Bellosi: *J. Eur. Ceram. Soc.*, 2007, vol. 27 (7), pp. 2729–39.
13. W.W. Wu, G.J. Zhang, Y.M. Kan, and P.L. Wang: *J. Am. Ceram. Soc.*, 2008, vol. 91 (8), pp. 2501–08.
14. J.M. Lonergan, W.G. Fahrenholtz, and G.E. Hilmas: *J. Am. Ceram. Soc.*, 2015, vol. 98 (8), pp. 2344–51.
15. L. Rangaraj, S.J. Suresha, C. Divakar, and V. Jayaram: *Metall. Mater. Trans. A*, 2008, vol. 39A, pp. 1496–05.
16. N. Chidambaram, L. Rangaraj, C. Divakar, and V. Jayaram: *J. Am. Ceram. Soc.*, 2010, vol. 93 (5), pp. 1341–46.
17. L. Rangaraj, C. Divakar, and V. Jayaram: *J. Eur. Ceram. Soc.*, 2010, vol. 30 (1), pp. 129–38.
18. L. Rangaraj, C. Divakar, and V. Jayaram: *J. Eur. Ceram. Soc.*, 2010, vol. 30 (15), pp. 3263–66.
19. S. Guo: *J. Eur. Ceram. Soc.*, 2014, vol. 34 (3), pp. 621–32.
20. D. Brodkin, S.R. Kalidindi, M.W. Barsoum, and A. Zavaliangos: *J. Am. Ceram. Soc.*, 1996, vol. 79 (7), pp. 1945–52.
21. M.W. Barsoum and B. Houng: *J. Am. Ceram. Soc.*, 1993, vol. 76 (6), pp. 1445–51.
22. T. Chakrabarti, L. Rangaraj, and V. Jayaram: *J. Am. Ceram. Soc.*, 2014, vol. 97 (10), pp. 3092–4002.
23. T. Chakrabarti, L. Rangaraj, and V. Jayaram: *J. Mater. Res.*, 2015, vol. 30 (12), pp. 876–86.
24. L. Rangaraj, T. Chakrabarti, K. Rajaguru, and V. Jayaram: *J. Mater. Res.*, 2016, vol. 31 (4), pp. 506–15.
25. J.K. Chakravartty, Y.V.R.K. Prasad, and M. Asundi: *Metall. Mater. Trans. A*, 1991, vol. 22A, pp. 829–36.
26. P. Zwigl and D.C. Dunand: *Metall. Mater. Trans. A*, 1998, vol. 29A, pp. 2571–82.
27. P.M. Sargent and M.F. Ashby: *Scripta Metall.*, 1982, vol. 16 (12), pp. 1415–22.
28. Z.A. Munir: *Am. Ceram. Soc. Bull.*, 1988, vol. 67 (2), pp. 342–49.
29. K. Niihara, R. Morena, and D.P.H. Hasselman: *J. Mater. Sci. Lett.*, 1982, vol. 1 (1), pp. 13–16.
30. J.S. Lannin: *Solid State Commun.*, 1978, vol. 25 (6), pp. 363–66.
31. H. Werhelt, V. Fillpov, U. Kuhlmann, U. Schwarz, M. Armbruster, A.L. Jasper, T. Tanaka, I. Higashi, T. Lundstrom, V.N. Gurin, and M.M. Korsukova: *Sci. Technol. Adv. Mater.*, 2010, vol. 11 (2), pp. 1–27.
32. A. Jain, C. Ghosh, T.R. Ravindran, S. Anthonysamy, R. Divakar, E. Mohandas, and G.S. Gupta: *Bull. Mater. Sci.*, 2013, vol. 36 (7), pp. 1323–29.
33. R. Kannan, K. Venkateswarlu, and L. Rangaraj: *Int. J. Appl. Ceram. Technol.* (in press).
34. A.I. Gusev, A.A. Rempel, and A.J. Magerl: *Springer Series in Materials Science*, Springer, New York, 2001.
35. D. Agaogullari, H. Gorce, I. Duman, and M.L. Ovecoglu: *J. Eur. Ceram. Soc.*, 2012, vol. 32 (7), pp. 1447–55.
36. A.W. Weimer: *Carbide, Nitride and Boride Materials Synthesis and Processing*, Chapman and Hall Publications, London, 1997, p. 643.
37. T. Tsuchida and S. Yamamoto: *J. Eur. Ceram. Soc.*, 2004, vol. 24 (1), pp. 45–51.